

Revisiting a many-body model for water based on a single polarizable site: From gas phase clusters to liquid and air/liquid water systems

Florent Réal, Valérie Vallet, Jean-Pierre Flament, and Michel Masella

Citation: *J. Chem. Phys.* **139**, 114502 (2013); doi: 10.1063/1.4821166

View online: <http://dx.doi.org/10.1063/1.4821166>

View Table of Contents: <http://jcp.aip.org/resource/1/JCPSA6/v139/i11>

Published by the **AIP Publishing LLC**.

Additional information on *J. Chem. Phys.*

Journal Homepage: <http://jcp.aip.org/>

Journal Information: http://jcp.aip.org/about/about_the_journal

Top downloads: http://jcp.aip.org/features/most_downloaded

Information for Authors: <http://jcp.aip.org/authors>

ADVERTISEMENT



**SHARPEN YOUR
COMPUTATIONAL
SKILLS.**

Subscribe for
\$49 | year

Computing
in **SCIENCE & ENGINEERING**
Scientific
Computing
with GPUs

Revisiting a many-body model for water based on a single polarizable site: From gas phase clusters to liquid and air/liquid water systems

Florent Réal,¹ Valérie Vallet,¹ Jean-Pierre Flament,¹ and Michel Masella²

¹Université de Lille 1, Laboratoire PhLAM, CNRS UMR 8523, CNRS FR 2416, Bât P5, F-59655 Villeneuve d'Ascq Cedex, France

²Laboratoire de Chimie du Vivant, Service d'ingénierie moléculaire des protéines, Institut de biologie et de technologies de Saclay, CEA Saclay, F-91191 Gif sur Yvette Cedex, France

(Received 29 June 2013; accepted 29 August 2013; published online 18 September 2013)

We present a revised version of the water many-body model TCPE [M. Masella and J.-P. Flament, *J. Chem. Phys.* **107**, 9105 (1997)], which is based on a static three charge sites and a single polarizable site to model the molecular electrostatic properties of water, and on an anisotropic short range many-body energy term specially designed to accurately model hydrogen bonding in water. The parameters of the revised model, denoted TCPE/2013, are here developed to reproduce the *ab initio* energetic and geometrical properties of small water clusters (up to hexamers) and the repulsive water interactions occurring in cation first hydration shells. The model parameters have also been refined to reproduce two liquid water properties at ambient conditions, the density and the vaporization enthalpy. Thanks to its computational efficiency, the new model range of applicability was validated by performing simulations of liquid water over a wide range of temperatures and pressures, as well as by investigating water liquid/vapor interfaces over a large range of temperatures. It is shown to reproduce several important water properties at an accurate enough level of precision, such as the existence liquid water density maxima up to a pressure of 1000 atm, the water boiling temperature, the properties of the water critical point (temperature, pressure, and density), and the existence of a “singularity” temperature at about 225 K in the supercooled regime. This model appears thus to be particularly well-suited for characterizing ion hydration properties under different temperature and pressure conditions, as well as in different phases and interfaces. © 2013 AIP Publishing LLC. [<http://dx.doi.org/10.1063/1.4821166>]

I. INTRODUCTION

Despite the huge efforts devoted to develop a universal model able to accurately describe water under different conditions and in different environments, see, for instance, the 27 models reviewed recently by Kiss and Baranyai,¹ building up a model able to describe the properties of water from gas phase to condensed phase still remains a major challenge in the microscopic simulation field. Recently, several new models have been proposed, which pave the road towards a universal model for water. Among them, we may quote in particular the polarizable models TTM n -F ($n = 2-3$),^{2,3} DPP2,⁴ HBB2-pol,⁵ SWM6,⁶ and BK3.⁷ Because of their sophistication and because of the very accurate strategy used to assign their parameters, these models were shown to accurately describe stable water clusters in gas phase, liquid water at ambient conditions, as well as under a wide range of temperatures, and even the water liquid/vapor interface, in the particular cases of BK3⁷ and SWM6.⁶ However, all these models are computationally demanding. For instance, they consider from three (DDP2, TTM n -F, HBB2-pol, and BK3) up to six (SWM6) polarizable sites per molecule to describe the water molecular electrostatic properties. To further improve the model accuracy, we may also note that specific classical energy terms have been altered in the above models, like the standard Coulombic term modified to account for charge-

charge penetration effects in DPP2 and BK3, and/or additional energy terms were introduced, like the charge transfer one of DPP2 or the energy term of HBB2-pol based on a linear combination of 27 exponential functions.⁵

Hence, developing an accurate, however, still computationally efficient water model remains an important challenge, especially to simulate large enough systems allowing to study the behavior of hydrated salts in bulk water and/or at the water liquid/vapor interface under different conditions, which have been recently further investigated using femtosecond infrared experimental techniques,⁸ for instance. In particular, because of the uncertainties affecting all the available models used to describe water/water and ion/water systems at the microscopic level, Netz and Horinek concluded in a recent review⁹ that all the simulation results presented to date concerning the behavior at the liquid/vapor interface even of simple ions such as halides, see, among others, Refs. 10–13 and the references cited therein, are not accurate enough to draw a clear picture of the latter phenomenon, in particular, in terms of their physical origin. In line with the latter conclusion, we recently exhibited^{14,15} that most of the efficient water models proposed so far have to fail in describing accurately the repulsive water/water interactions taking place in the first hydration shell of multi-charged ions, such as the heavy ones Th(IV) and Cm(III), which play a key role in the nuclear waste energy field.

Our aim here is to propose a revised (and rigid) version of the efficient many-body model for water, TCPE,¹⁶ which was originally developed to model water clusters in gas phase. The TCPE model is based on a static three-site electrostatic charge set and on a single polarizable site, coinciding with the water oxygen, to model the molecular electrostatic properties of water. As this kind of models is based on a single polarizable site, we exhibited that they are well suited to be used in conjunction with a multiple-time steps algorithm¹⁷ to solve the Newtonian equations of motion, in order to efficiently generate molecular dynamics (MD) trajectories. However, models based on such a simple approach are well known to be unable to provide an accurate description of water both in gas and in condensed phases. Hence, as soon as the original version of the TCPE model was presented, we introduced a short range many-body anisotropic potential, which allows us for an accurate description of water hydrogen bond networks.¹⁶ Note that the global efficiency of the TCPE approach also originates from the truncation of the latter energy term, typically at a water hydrogen bond distance of 6 Å.

In 2008, we proposed a first revision of the original TCPE model, in order to simulate water clusters in gas phase as well as liquid water at ambient conditions.¹⁸ Hereafter, the original TCPE model and its first revision are denoted TCPE/1997 and TCPE/2008, respectively. By using the model TCPE/2008, we showed that the electrostatic properties of water at the close vicinity of an ion in liquid water, as computed from quantum approaches, can be reproduced by considering only a single polarizable site per water molecule.^{15,19} However, TCPE/2008 largely overestimates the repulsive character of water/water interactions in the first hydration shell of multi-charged ions,^{14,15} suggesting that our first encouraging results derived from that model and concerning the solvation of such ions, can be the results of large cancellation of errors. Hence, the transferability of that model to the study of salt solutions under various conditions, for instance, is questionable. As already mentioned above, this remark applies to all the efficient water models proposed to date.

In the present study, we present a new revised version of the TCPE model, called TCPE/2013, which has been developed to accurately model the properties of water clusters in gas phase, as well as the repulsive interactions occurring in the water structures observed in cation first hydration shells. Here, we consider only the properties computed using high level quantum methods, in particular, at the complete basis set (CBS) limit. However, as only an overall reduced set of high quality quantum computations concerning water clusters have been reported, we have finely tuned up a reduced set of the TCPE/2013 parameters, e.g., those handling water/water interactions at medium range, to reproduce two properties of liquid water at ambient conditions, namely, the water vaporization enthalpy and density. As compared to the TCPE/1997 original approach, we have here revised the analytical form of the TCPE short range anisotropic many-body energy term, and we have re-assigned most of the model parameters. We show that the revised TCPE/2013 model is now able to accurately model water clusters in gas phase (with a precision close to that of the recent HHB2-pol model⁵) as well as most of the properties of liquid water and of the liquid/vapor in-

terface under different temperature and pressure conditions. As this new model also thoroughly describes the repulsive water/water interactions in multi-charged cation first hydration shells, it appears to be particularly well suited to investigate heavy ion properties in aqueous phase and at water liquid/vapor interfaces.

Concerning the above mentioned repulsive water/water interactions in cation first hydration shell, we also investigated them at the MP2/CBS limit. The quantum protocol used and the results will be here also briefly presented and commented.

II. THE REVISED TCPE/2013 MODEL

All model computations have been performed using our own simulation code POLARIS(MD), whose several features are described hereafter.

A. The standard potential energy terms

The TCPE approach is based on the following decomposition of the potential energy

$$U = U^{rep} + U^{qq'} + U^{pol} + U^{rel} + U^{hb}. \quad (1)$$

The individual terms correspond, respectively, to the repulsive term, the classical pairwise Coulombic term, the polarization term, the intramolecular relaxation term (describing the interactions among chemically bonded atoms), and the hydrogen bonded term, which represents the main originality of the TCPE approach. In the following, all the intermolecular energy terms sum interactions between atoms that are not chemically bonded. These sums are denoted by the superscript *.

For a system made of N atoms, the intermolecular repulsive term is a radial pairwise energy term

$$U^{rep} = \sum_{i=1, N, j>i}^* A_{ij} \exp(-B_{ij}r_{ij}), \quad (2)$$

where A_{ij} and B_{ij} are two parameters depending on the chemical nature of the atoms i and j , and r_{ij} is the distance between these atoms. To model oxygen-hydrogen repulsion interactions, the above pre-exponential factor A is altered so that U^{rep} corresponds to a many-body potential energy term. It will be described in Sec. II B.

The Coulombic term is the standard additive potential

$$U^{qq'} = \frac{1}{4\pi\epsilon_0} \sum_{i=1, N, j>i}^* \frac{q_i q_j}{r_{ij}}, \quad (3)$$

where q_i and q_j are static point charges located on atomic centers. Originally, they were defined to reproduce the dipole moment of a water molecule in gas phase (1.85 D). For TCPE/2013, they are defined to best reproduce both the latter dipole moment and the interaction energies of water molecules interacting in cation first hydration shells.

The term U^{pol} is introduced to account for polarization effects, described by means of a set of induced point dipole moments $\{\mu_i\}_{i=1, N_\mu}$ located on a subset of N_μ atomic centers.

They obey

$$\boldsymbol{\mu}_i = \alpha_i \cdot \left(\mathbf{E}_i^q + \sum_{j=1, N_\mu, j \neq i}^* \mathbf{T}_{ij} \boldsymbol{\mu}_j \right). \quad (4)$$

Here, α_i is the isotropic polarizability of the polarizable atom i , \mathbf{E}_i^q is the electric field generated on i by the surrounding static charges q_j , and \mathbf{T}_{ij} is the dipolar tensor. The corresponding polarization energy term is defined as

$$U^{pol} = \frac{1}{2} \sum_{i=1}^{N_\mu} \frac{\mu_i^2}{\alpha_i} - \sum_{i=1}^{N_\mu} \boldsymbol{\mu}_i \cdot \mathbf{E}_i^q - \frac{1}{2} \sum_{i=1}^{N_\mu} \sum_{j=1, j \neq i}^{N_\mu} \boldsymbol{\mu}_i \mathbf{T}_{ij} \boldsymbol{\mu}_j, \quad (5)$$

and the dipolar tensor is defined as

$$\mathbf{T}_{ij} = \frac{1}{4\pi\epsilon_0} \left(\frac{f_5(r_{ij})}{r_{ij}^5} \begin{bmatrix} x^2 & xy & xz \\ xy & y^2 & zy \\ zx & zy & z^2 \end{bmatrix} - \frac{f_3(r_{ij})}{r_{ij}^3} \mathbf{I}_3 \right). \quad (6)$$

Here, x , y , and z are the coordinates of the vector connecting the polarizable centers i and j , and \mathbf{I}_3 is the identity matrix. The functions f_5 and f_3 are introduced to account for short range damping effects. They are defined by following the original ideas of Thole²⁰ and by considering the radial charge density

$$\rho(r) = \frac{3a}{4\pi} \exp(-ar^3), \quad (7)$$

where a is a parameter. This leads to

$$f_3(r_{ij}) = 1 - \exp(-a_{ij}r_{ij}^3), \quad (8)$$

$$f_5(r_{ij}) = 1 - (1 + a_{ij}r_{ij}^3) \exp(-a_{ij}r_{ij}^3). \quad (9)$$

Here, a_{ij} is a parameter depending on the nature of the atoms i and j . Note that the function f_3 is also used to scale the individual components of the static electric field \mathbf{E}_i^q acting on each polarizable site i . In the TCPE approach, the polarizable atoms are not sensitive to the electric fields generated by the atoms to which they are chemically bonded. Hence, the parameter a_{ij} are not defined to reproduce molecular electrostatic properties, as originally proposed by Thole.²⁰ They are assigned to reproduce only energetic properties (such as binding energies of small molecular aggregates) together with the other model parameters.

Only the water oxygen atoms are polarizable sites for TCPE (their isotropic polarizability is set to the water ex-

perimental value in gas phase, e.g., 1.45 Å³). Regardless of the computations performed (like optimizations in gas phase or MD trajectories), the induced dipole moments are solved iteratively, until an averaged convergence criterion of 10⁻⁶ D per polarizable site is reached. However, the iterative process goes on until the maximum deviation for a single dipole moment between two successive iterations is smaller than 5 × 10⁻⁶ D.

Finally, the intramolecular term U^{rel} is based on standard harmonic potentials to handle the OH stretching and the HOH bending degrees of freedom. In the present study, our aim is to build up a rigid model for water, and we impose the water geometry to correspond to that of a water molecule in liquid phase, at ambient conditions, e.g., $r(\text{OH}) = 0.97$ Å and $\angle \text{H} - \text{O} - \text{H} = 106.0^\circ$.²¹ Hence, we use common algorithms to remove the incidence of U^{rel} in our computations, and it will be thus not further discussed.

B. The hydrogen bond term

The hydrogen bond term U^{hb} is introduced to accurately model the interactions among water molecules, as defined in small water clusters. It is based on a many-body anisotropic potential¹⁶

$$U^{hb} = \sum F(r_{hb}) \times G(\theta, \phi). \quad (10)$$

Here, the sum runs over all the hydrogen bond pairs, which can be defined in a water cluster. r_{hb} is the hydrogen bond length. The angle θ may be interpreted as the angle between one water lone pair and the O–H bond of the second water molecule participating to the hydrogen bond, whereas ϕ is the $\angle \text{O} \cdots \text{H} - \text{O}$ angle (see Figure 1). G is an additive function defined as

$$G(\theta, \phi) = \exp(-(\theta - \theta_e)^2/\gamma_\theta) \times \exp(-(\phi - \phi_e)^{n_\phi}/\gamma_\phi). \quad (11)$$

Here, γ_θ and γ_ϕ are two parameters. In the original TCPE approach,¹⁶ n_ϕ was set to 2. In the present revised model, n_ϕ is set to 4. That allows us for an overall better description of small water aggregates.

The many-body radial component F obeys

$$F(r_{hb}) = -D_e \times f_{hb}(r_{hb}, r_{hb}^e, \gamma_r, R_c) \quad (12)$$

with $f(r_{hb}, r_{hb}^e, \gamma_r, R_c)$ defined as

$$f_{hb}(r_{hb}, r_{hb}^e, \gamma_r, R_c) = \begin{cases} 0 & \text{if } r_{hb} \geq R_c \\ \exp(-(r_{hb} - r_{hb}^e)^2/\gamma_r) \times P_5(r_{hb}, r_{hb}^e, R_c) & \text{if } R_c > r_{hb} > r_{hb}^e, \\ 1 & \text{if } r_{hb} \leq r_{hb}^e \end{cases}, \quad (13)$$

where r_{hb}^e , γ_{hb} , and R_c are three parameters ($R_c > r_{hb}^e$). $P_5(r_{hb}, r_{hb}^e, R_c)$ is a five order polynomial-based function, which is equal to zero for $r_{hb} \geq R_c$, to 1 for $r_{hb} \leq r_{hb}^e$, and, otherwise, to

$$P_5(r_{hb}, r_{hb}^e, R_c) = 1 - 10 \left(\frac{r_{hb} - r_{hb}^e}{R_c - r_{hb}} \right)^3 + 15 \left(\frac{r_{hb} - r_{hb}^e}{R_c - r_{hb}} \right)^4 - 6 \left(\frac{r_{hb} - r_{hb}^e}{R_c - r_{hb}} \right)^5. \quad (14)$$

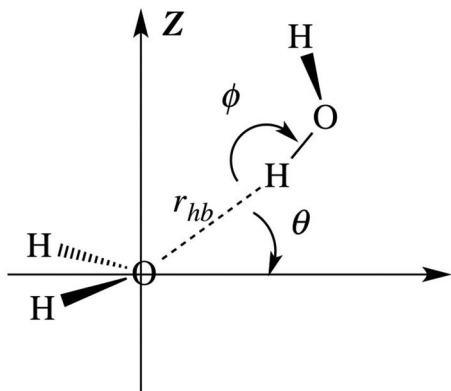


FIG. 1. Definition of the geometrical parameters r_{hb} , θ and ϕ of the energy term U^{hb} . The axis X is the bisector of the angle $\angle\text{H-O-H}$ of the water molecule whose oxygen accepts the hydrogen atom in a hydrogen bond. The axis Z is orthogonal to the plane HOH of the latter water molecule.

We account for the incidence of the chemical environment on the magnitude of a specific $\text{water}_1/\text{water}_2$ hydrogen bond by taking D_e as a function of the water local density at the vicinity of the molecule water_1 , i.e., the molecule whose oxygen is involved in the latter hydrogen bond. The water local density is defined in terms of the number n_b of hydrogen bonds involving the hydrogen atoms of the molecule water_1

$$n_b = \sum f_{hb}(r_{hb}, r_{hb}^e, \gamma'_{hb}, R_c), \quad (15)$$

where r_{hb} , r_{hb}^e , and R_c are defined as above, γ'_{hb} is an adjustable parameter. The sum runs over all the hydrogen bonds, which may be defined between the water_1 hydrogens and water molecules $\neq \text{water}_2$. In the original TCPE/1997 approach, D_e was taken as a linear function of n_b

$$D_e = d_e \times (1 + \xi_b n_b), \quad (16)$$

where d_e and ξ_b being two adjustable parameters (note that $D_e = d_e$ for the water dimer). In the revised TCPE/2013 approach, we allow D_e to saturate according to

$$D_e = d_e \times (1 + \xi_b n_{max}^{hb} \ell(3n_b/n_{max}^{hb})), \quad (17)$$

where $\ell(x) = \coth(x) - 1/x$ denotes the Langevin function. The saturation parameter n_{max}^{hb} is set here arbitrarily to 2, e.g., the ideal value expected in bulk water.

In the original version of TCPE,¹⁶ r_{hb}^e was also a linear function of n_b . This was introduced to account for the strong incidence of cooperative effects not only on the energetic of water clusters, but also on their geometry (see, for instance, the discussions provided in Ref. 22). In the revised TCPE/2013 model, we consider an alternative approach to account for the many-body effects on water hydrogen bond lengths. Instead of altering r_{hb}^e , we alter here the component $u^{rep}(\text{O}, \text{H})$ of the term U^{rep} handling the oxygen/hydrogen repulsive interaction in a hydrogen bond as follows:

$$u^{rep}(\text{O}, \text{H}) = A_{(\text{O}, \text{H})} \times (1 - \xi_{rep} n_{max}^{hb} \ell(3n_b/n_{max}^{hb})) \times \exp(-B_{(\text{O}, \text{H})} \cdot r_{(\text{O}, \text{H})}), \quad (18)$$

where $A_{(\text{O}, \text{H})}$ and $B_{(\text{O}, \text{H})}$ are the parameters A_{ij} and B_{ij} defined in Eq. (2), $r_{(\text{O}, \text{H})}$ is the hydrogen bond length and ξ_{rep}

is an adjustable parameter. Hence, we consider now a repulsive many-body energy term for handling specifically the oxygen-hydrogen short repulsion effects in water systems. Such an approach can be interpreted as accounting for the water electronic density alteration induced by the water chemical environment.

The aim TCPE/2013 is also to best reproduce the interaction energies for water molecules interacting in geometries corresponding to those observed in cation first hydration shells. As it will be discussed hereafter, this is achieved by lowering the strong repulsive character of the water/water interactions in such situations. However, from our own numerical experiments, this introduces an artifact when using the revised TCPE approach to model large and stable water aggregates: up to four water hydrogen atoms can then interact with a single water oxygen. One way to remediate this artifact is to introduce a new component to the term U^{hb} , whose aim is to alter the stabilizing character of U^{hb} when more than 2 water hydrogens interact with a single oxygen atom at short range. Thus, the revised hydrogen bonding term is $U^{hb} + U_{rep}^{hb}$, where the new component, U_{rep}^{hb} , is defined as

$$U_{rep}^{hb} = D_e^c \sum_{i=1}^{N_w} \sum_{H(j), j \neq i} \sum_{H(k), k > j} \times \frac{f_{hb}(r_j^{hb}, r_{hb}^e, \gamma_r, R_c^*) \times f_{hb}(r_k^{hb}, r_{hb}^e, \gamma_r, R_c^*)}{1 + \delta \exp(-Z_j Z_k)}. \quad (19)$$

Here, δ is an adjustable parameter, N_w is the number of water molecules, and $H(j)$ denotes the hydrogen atoms of the water molecule j . Z_j and Z_k are the projections on the axis Z of the water molecule i , of the vectors \mathbf{r}_j^{hb} and \mathbf{r}_k^{hb} connecting the hydrogen atoms of the molecules j and k to the oxygen of the molecule i (see Figure 2). D_e^c is tied to the U^{hb} parameter d_e , according to $D_e^c = (1 + n_{max}^{hb} \xi_b) \times d_e$. As d_e and ξ_b are both > 0 , U_{rep}^{hb} is a pure repulsive energy term, preventing the hydrogens of two water molecules to interact with the

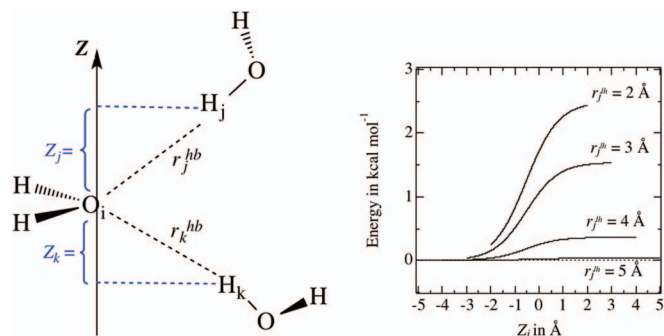


FIG. 2. (Left) Definition of the water axis Z , and of the projections Z_j and Z_k of the hydrogen bond vectors \mathbf{r}_j^{hb} and \mathbf{r}_k^{hb} of the latter axis. Z is orthogonal to the plane defined by the water molecule i and it is centered at the oxygen O_i . Hence, here $Z_j > 0$ and $Z_k < 0$. (Right) $U_{rep}^{hb}(Z_j)$ profiles for the water system shown on the left and for different r_j^{hb} hydrogen bond lengths, included within 2 and 5 Å. Here, we consider both Z_k and r_k^{hb} as fixed parameters set to 1.5 Å and 2.0 Å, respectively. The parameters of U_{rep}^{hb} used here are those summarized in Table I.

same oxygen atom of a third water molecule i , within the same space domain defined by the plane of molecule i . U_{rep}^{hb} scales *a priori* as $O(N_w^3)$. However, because of the analytical form of the function $f(r_{hb}, r_{hb}^e, \gamma_r, R_c^*)$, it scales as $O(N_w)$. The same conclusion holds for the term U^{hb} .

The energy term U^{hb} was originally introduced to accurately reproduce a key property of water hydrogen bonding when using a simple polarizable model for water, e.g., the reinforcement of water hydrogen bond networks when water molecules act simultaneously as donor and acceptor of hydrogen bonds. Because of its analytical form, one may consider that this term is introduced to account for possible charge transfer effects occurring in water hydrogen bonds. However, because of the lack of a standard R^{-6} term in the TCPE approach, the term U^{hb} allows us to account also for dispersion interactions. Note that the accurate modeling of water dispersion interactions requires to consider different types of interactions (usually, oxygen-oxygen, oxygen-hydrogen, and hydrogen-hydrogen ones, see Ref. 23, for instance). This suggests the total water/water dispersion energy to present also an anisotropic character.

C. Assignment of the model parameters

Unlike the original model TCPE/1997,¹⁶ the first step in the TCPE/2013 parameter assignment was to define the U^{rep} parameters (with the exception of the parameter ξ_{rep}), as well as the oxygen and hydrogen static electrostatic charges, in order to best reproduce the gas phase dipole moment of water, the quantum equilibrium geometry of the global minimum of the water dimer (in terms of oxygen-oxygen distance) and the interaction energies corresponding to water molecules in the first hydration shell of a multi-charged cation, here Th(IV). For the present purpose, Th(IV) is particularly well suited, since it can host up to ten water molecules in its first coordination sphere.^{14,29,30} The reference dimer geometry is the one reported in Ref. 24, optimized at the CCSD(T)/TZ2P(f, d) + diffuse level of theory. The data concerning the hydrated cation are derived from our own computations performed at a high level of theory (see the supplementary material⁸³).

Once the above first set of parameters are assigned, we followed a protocol close to the TCPE/1997 original one,¹⁶ e.g., the remaining parameters are assigned to reproduce the binding energies of the global minimum and of three remarkable stationary points of the water dimer potential energy surface, e.g., the stationary points labelled **3**, **4**, and **9** in Ref. 25, as well as the cyclic water trimer binding energy and geometry. For the cyclic water trimer, we consider the reference mean oxygen-oxygen distance to be 2.83 Å, which corresponds to the upper bound of quantum estimates (see below), and which is smaller by 0.02 Å as compared to the VRT-based experimental estimate.²²

However, we also consider an additional condition to be met, e.g., to reproduce the energy ordering of the water hexamers *prism*, *cage*, and *cyclic* (see the supplementary material⁸³), as reported from MP2 computations at the CBS limit.²⁶⁻²⁸ Most of the U^{hb} parameters are assigned from dimer and cyclic trimer quantum data. The U_{rep}^{hb} parameter δ is adjusted from the hexamer data, and the damping parameter a_{OH} is adjusted by considering all the above mentioned cluster data. We tested several values for the damping parameter a_{OO} , in the expected range of values, which is included within 0.2 and 0.5 Å⁻³. However, the incidence of its value on water cluster results is almost negligible in the latter range. Hence, we set it arbitrarily to 0.3 Å⁻³.

Assigning the model parameters from the above set of water clusters does not allow us to fine tune them for an accurate description of water/water interactions corresponding to inter-oxygen distances larger than 4 Å. As these interactions play a key role in microscopic simulations to accurately reproduce the properties of liquid water at ambient conditions, we refined the parameters γ_{hb} and γ_r of the terms U^{hb} and U_{rep}^{hb} , respectively, to best reproduce the experimental values of the liquid water density and vaporization enthalpy at ambient conditions. The latter properties were estimated from NPT MD simulations of a water box comprising 1000 molecules and simulated using periodic boundary conditions (see below for details). Finally, three TCPE/2013 parameters corresponding to the energy terms U^{hb} and U_{rep}^{hb} are fixed arbitrarily, mainly from efficiency considerations, i.e., the cutoff distances R_c and R_c^* and the parameter γ'_{hb} . All the TCPE/2013 parameters are summarized in Table I.

TABLE I. Parameters of the TCPE/2013 model.

Energy term	Unit	Parameter	Value	Parameter	Value	Parameter	Value
$U^{qq'}$	e	q_O	-0.64350	q_H	0.32175		
U^{pol}	Å ³	α_O	1.45				
	Å ⁻³	a_{OO}	0.300	a_{OH}	0.259		
U^{rep}	kcal mol ⁻¹	A_{OO}	60 000	A_{OH}	68 000	A_{HH}	60 000
	Å ⁻¹	B_{OO}	4.915	B_{OH}	5.770	B_{HH}	7.000
	Å ⁻²	ξ_{rep}	0.056				
$U^{hb} + U_{rep}^{hb}$	kcal mol ⁻¹	d_e	1.56				
	Å ⁻²	γ_{hb}	2.80	γ'_{hb}	0.15	γ'	0.268
	Å	r_{hb}^e	1.94				
	deg	θ_e	54.0	ϕ_e	0.0		
	rad ⁻²	γ_θ	0.70	γ_ϕ	0.75		
	...	ξ_b	0.335	δ	0.450	n_{max}^{hb}	2.0
	Å	R_c	6.25	R_c^*	4.00		

III. MD SIMULATION AND TRAJECTORY ANALYSIS DETAILS

A. Simulations in liquid phase

MD simulations in condensed phase were performed by considering periodic boundary conditions and standard Ewald summation techniques (the direct and reciprocal energy terms were truncated based on a medium Ewald sum precision, e.g., 10^{-6} , see Ref. 31). We also reperformed most of our simulations using the SPME method.³² In the latter case, the direct term cutoff distance was set to 12 Å, the expansion of the B-spline functions was set to 8, and we generate two series of trajectories corresponding to two different interpolation grids, made of 32^3 and 64^3 nodes, respectively. Regardless of the Ewald techniques used, no surface term was considered (that corresponds to infinite tinfoil conditions). All the MD data discussed below correspond to standard Ewald simulations. The differences with SPME results are negligible, whatever the interpolation grid dimension (see data summarized in the supplementary material⁸³).

The Newtonian equations of motion were solved using the multiple time steps r-RESPAP algorithm,¹⁷ with two time steps: 1 fs for short range inter-molecular interactions (including U^{rep} and $U^{hb} + U_{rep}^{hb}$), and 5 fs for the remaining long-range electrostatic interactions. For NVT simulations, we used the generalized Gaussian moment thermostat,³³ and for NPT ones, the Nosé-Hoover barostat.³⁴ The water O–H bonds and $\angle H - O - H$ angles were both restrained to their equilibrium values using the iterative RATTLE procedure, regardless of the thermodynamic ensemble considered (the convergence criterion was set to 10^{-6} Å).

At the exception of free energy computations (see below), liquid water was simulated by considering a cubic box made of 1000 water molecules. The MD simulations were performed at the 10 ns scale, and their last 9 ns segments were sampled each 1 ps to compute the statistical averages (note that the uncertainties affecting our MD averages were estimated from a basic block averaging method, see the supplementary material⁸³).

B. Thermodynamic properties of water in liquid phase

The water enthalpy of vaporization is estimated according to the standard relation

$$\Delta H_{vap}(T) = -\bar{u} + k_B T, \quad (20)$$

where \bar{u} is the system total mean potential energy per molecule along a trajectory.

The Gibbs free energy of vaporization, $\Delta G_{vap}(T)$, are computed using the classical free energy Thermodynamic Integration (TI) scheme, which is based on a linear interpolation of Hamiltonians. For our purpose, we select a water molecule, which is progressively decoupled from the other ones. For a water systems comprising N_w molecules, the different energy terms of Eq. (1) may be rewritten as a sum involving N_w energy components u^{rep} , $u^{qq'}$, u^{pol} , u^{hb} , and u^{rel} . The Hamiltonian handling the water molecule decoupled from the bulk

during the TI computations is here taken as

$$u(\lambda) = u^{rel} + g(\lambda) \times (u^{rep} + u^{hb}) + h(\lambda) \times (u^{qq'} + u^{pol}), \quad (21)$$

where g and h are two linear functions of the TI parameter λ monitoring the decoupling of the water molecule from the bulk: $g(\lambda) = 1 - \lambda$ and $h(\lambda) = \max(1 - 2\lambda, 0)$. Such a protocol is close to the two steps decoupling scheme proposed by Shirts and Pande.³⁵ Note that, as soon as $\lambda = 0.5$, the water molecule decoupled from the bulk is no more accounted for when updating the atom neighbor list used to efficiently compute the direct term in Ewald-based MD approaches.

Here, we consider a twenty steps TI scheme. Each step corresponds to a trajectory of a water box made of 1000 molecules, simulated using periodic boundary conditions. The trajectory duration is 2.5 ns. The last 2 ns of each trajectory is sampled each 250 fs to compute the statistical averages. The free energies computed according to that protocol, $\Delta G_{sim}(T)$, are used to approximate the $\Delta G_{vap}(T)$ according to the standard relation

$$\Delta G_{vap}(T) = k_B T \ln \left(\frac{P}{\rho_l k_B T} \right) + \Delta G_{sim}(T), \quad (22)$$

where ρ_l is the density of liquid water at temperature T and pressure P . From the value $\Delta G_{vap}(T)$, we compute then the vapor pressure P_{vap} as follows:

$$P_{vap}(T) = P \exp(-\Delta G_{vap}(T)/k_B T). \quad (23)$$

C. Other liquid water properties

The liquid water structure is discussed in terms of standard radial distribution functions, namely the oxygen-oxygen one, $g_{OO}(r)$, the oxygen-hydrogen one, $g_{OH}(r)$, and the hydrogen-hydrogen one, $g_{HH}(r)$, as well as in terms of water coordination numbers corresponding to the first and second water oxygen hydration shells, as computed by integrating the latter distribution functions.

Water transport properties, in terms of self-diffusion coefficients, D_{sim} , are computed from the Einstein equation

$$D_{sim} = \lim_{t \rightarrow \infty} \frac{\langle |\mathbf{r}(t) - \mathbf{r}(0)|^2 \rangle}{6t}, \quad (24)$$

where t is the simulation time and the molecular vector positions \mathbf{r} are measured by considering the water center of mass located on the water oxygen. When using periodic boundary conditions, the above coefficients D_{sim} have to be corrected to account for the finite size of the simulation cell. This is achieved here by performing different 10 ns MD simulations, at $P = 1$ atm, of a set of water cubic boxes whose size is L^3 , and which comprises 216, 343, 512, 1000, and 1728 water molecules, respectively. As shown by Yeh and Hummer,³⁶ the D_{sim} values are tied to the dimensions L according to

$$D_{sim} \approx D_{\infty} - \frac{\xi k_B T}{6\pi\eta L}. \quad (25)$$

Hence, from the above set of MD simulations, one may estimate both a diffusion coefficient D_{∞} , which may be compared

to experiment, as well as the water shear viscosity η (ξ is a parameter, whose value is 2.837297³⁶).

As we simulated liquid water under a large set of temperature and pressure conditions, we compute the thermal-expansion coefficient α_P , by fitting first the water densities ρ under different pressures to a five order polynomial function of T , denoted $\rho_P^{poly}(T)$. Then we compute α_P from the standard relation

$$\alpha_P = - \left(\frac{\partial \ln \rho_P^{poly}(T)}{\partial T} \right)_P. \quad (26)$$

The isobaric heat capacity C_P , the isothermal compressibility κ_T , and the static dielectric constant ϵ_r of liquid water are computed according to the standard relations

$$C_P = \frac{\bar{H}^2 - \bar{H}^2}{k_B T^2}, \quad (27)$$

$$\kappa_T = \frac{\bar{V}^2 - \bar{V}^2}{\bar{V} k_B T}, \quad (28)$$

$$\epsilon_r = 1 + \frac{4\pi}{3\bar{V}k_B T} (\bar{M}^2 - \bar{M}^2), \quad (29)$$

where V , H , and M are the instantaneous volume, enthalpy, and total dipole moment of the simulation cell along a trajectory. From the value of M at time t , the Debye relaxation time τ_D is estimated from exponential fits of the decay of the autocorrelation function $C_M(t)$ defined as

$$C_M(t) = \frac{\langle \mathbf{M}(0) \cdot \mathbf{M}(t) \rangle}{\bar{M}^2}. \quad (30)$$

The mean residence time (*mrt*) of water molecules in the water oxygen first hydration shell is computed according to the scheme proposed by Impey *et al.*³⁷ From the probability survival function $p_i(t_0, t_0 + t; \tau^*)$ of the i th water molecule (equal to 1 if that molecule is present in the first hydration shell at both time steps t_0 and $t_0 + t$ and does not leave the coordination shell for any continuous period longer than τ^* , while it takes the value zero otherwise), we compute the correlation function

$$C(t) = \frac{1}{n_c^1} \left\langle \sum_{i=1}^{n(t_0)} p_i(t_0, t_0 + t; \tau^*) \right\rangle_{t_0}, \quad (31)$$

where $n(t_0)$ is the number of water molecules in the first hydration shell at time t_0 and n_c^1 the mean coordination number in water first hydration shell. The *mrt* is then computed by assuming

$$C(t) = n_c^1 \times \exp(-t/mrt). \quad (32)$$

For water molecules in water first hydration shell, the expected values of *mrt* are about 5 ps for liquid water at ambient conditions. For such small values, it is known that the approach proposed by Impey *et al.*³⁷ suffers from the high sensitivity of the computed *mrt* values to the choice of τ^* .³⁸ Hence, to draw meaningful conclusions, we compute the *mrt*s for different τ^* values, namely, 1, 2, and 4 ps.

D. Simulations of the air/water liquid interface

To get a reasonable starting structure to simulate water at the air/liquid interface and at a temperature T , we first generated a 1 ns NPT trajectory of a water box made of 2000 molecules and whose dimensions are $(L, L, 2L)$, using periodic boundary conditions ($P = 1$ atm). The average dimension \bar{L} corresponding to the last 100 ps segment of the trajectory was then computed and a new 1 ns NVT simulation was performed by considering the last structure of the latter trajectory and the cell dimension set $(\bar{L}, \bar{L}, 2\bar{L})$. Finally, the last point of the NVT trajectory was taken as the starting one of a 5 ns NVT simulation for which the cell dimensions are $(\bar{L}, \bar{L}, 6\bar{L})$. The simulated system presents thus two liquid/vapor interfaces.

From the last 4 ns segments of the air/liquid simulations, we computed the water density profiles $\rho(z)$ along the z -axis, which is orthogonal to the two air/liquid interfaces. The liquid and vapor densities ρ_l and ρ_v are then extrapolated according to the relation

$$\rho(z) = \frac{\rho_l + \rho_v}{2} + \frac{\rho_l - \rho_v}{2} \times \tanh(a_0(z - a_1)), \quad (33)$$

here, a_0 and a_1 are two parameters.

We computed the surface tension of liquid water at temperature T , $\gamma(T)$, from the test-area simulation method³⁹

$$\gamma(T) = \left(\frac{\Delta A}{\Delta S} \right)_{N,V,T}, \quad (34)$$

where ΔA is the change in the free energy for an infinitesimal change in the interfacial area S . Each $\gamma(T)$ was computed from a single 4 ns NVT trajectory segment of the air/liquid water system discussed above, according to a Free Energy Perturbation-like scheme, with the two perturbed states corresponding to an altered surface area $S_{\pm} = L_x L_y (1 \pm \delta_s)$. x and y are the two dimensions orthogonal to the z -axis mentioned above, and the perturbation is equally applied to both. As recommended by Vega and de Miguel, we set δ_s to 5×10^{-4} .⁴⁰

IV. RESULTS AND DISCUSSION

A. Water aggregates in gas phase

1. Gas phase water clusters $(H_2O)_n$, $2 \leq n \leq 10$

Concerning the water monomer, the static electrostatic charges derived from our parameter assignment strategy leads to a water permanent dipole moment in gas phase of 1.80 D, still in good agreement with the experimental value, 1.85 D.

Model and quantum estimates of the binding energies for several water clusters $(H_2O)_n$, $n = 2-10$ are summarized in Table II. The quantum data correspond to various CBS results,^{2,24,26-28} or to our own data, computed at the MP2/6-311+G(2df,2p) level,^{16,41} when no CBS values are available. Note the structures here considered for the decamer and 9-mer are the most stable ones reported by Temelso *et al.*²⁸ The TCPE/2013 results are in very good agreement with the CBS ones, regardless of the quantum data set considered. Such a good agreement between both kinds of theoretical methods is observed for the difference in the binding energies of water cluster isomers, in particular, those which were not

TABLE II. Comparison of TCPE/2013 $(\text{H}_2\text{O})_n$ energies, in kcal mol^{-1} , to available quantum MP2 and CCSD(T) estimates, extrapolated to the CBS limit (cluster geometries are shown in the supplementary material⁸³). In bold character, cluster binding energies, and otherwise, for cluster isomers, difference in binding energy between a given isomer and the most stable one. The columns refer to: (a) quantum data from Ref. 28; (b) quantum data from Refs. 2 and 26; (c) quantum data from Ref. 27; (d) quantum data from Ref. 28, with the exception of the data labeled ¹, taken from Ref. 24; (e) quantum data labelled ² from Ref. 16 and those labelled ³ from Ref. 41.

n		TCPE	$\text{MP2}_{\text{CBS}}^T$ (a)	$\text{MP2}_{\text{CBS}}^X$ (b)	$\text{MP2}_{\text{CBS}}^M$ (c)	CCSD(T)/CBS (d)	MP2 (e)
2	C_s	4.97	5.03	4.97	5.03	4.8	...
2	3	0.55	0.59 ¹	...
2	4	0.87	0.87 ¹	...
2	9	1.70	1.70 ¹	...
3	UUD	15.78	15.67	15.82	14.9	15.70	...
3	OP-1	6.79	7.01 ²
3	OP-2	8.57	8.89 ²
4	S4	25.80	27.63	27.63	26.8	27.43	...
4	CY-1	8.23	9.0 ³
4	CY-2	9.51	11.9 ³
4	PY	4.18	3.97	2.70	...
4	PY-2	3.80	6.0 ³
5	CY	34.87	36.39	36.31	36.3	36.0	...
5	FR-B	0.87	2.14	1.13	...
6	PR	44.50	46.01	45.86	45.3	46.14	...
6	CC	1.19	0.95	1.00	1.7	1.54	...
6	BK-1	1.14	0.26	0.15	...	0.63	...
6	CA	0.53	-0.01	0.07	0.3	0.21	...
7	PR1	54.9	57.4	...
8	S4	68.4	72.8	72.7	72.3	72.6	...
9	IX	78.3	81.7	...
10	X	89.9	92.9	...

taken into account to assign the model parameters. However, TCPE/2013 underestimates the binding energies of clusters larger than the trimer compared to MP2/CBS data, up to about 5% for the octamer S_4 . From the data corresponding to larger clusters, the TCPE/2013 binding energy underestimation decreases then, down to about 3% for the water decamer.

A set of eleven water heptamer isomers, characterized by different hydrogen bond networks, have been investigated by Temelso *et al.*²⁸ at a high level of quantum theory. In particular, the latter authors reported estimates, at the CCSD(T)/CBS level, of the binding energies for that full set of isomers. In Figure 3, we compare the difference in energies ΔE_7 between the most stable water heptamer, **PR1**, and the other ten ones, as reported at the latter quantum level of theory and by using TCPE/2013. The heptamers are here labelled as in Ref. 28, and the starting points for TCPE/2013 optimizations are the three-dimensional structures provided in the supplementary material⁸³ of the latter study. We note again a good agreement between both sets of ΔE_7 values. In particular, TCPE/2013 and CCSD(T)/CBS computations predict the same three water heptamers, namely, **PR1**, **PR2**, and **PR3**, to be the most stable ones, their ΔE_7 values differing at most by $0.5 \text{ kcal mol}^{-1}$, regardless of the theoretical method used. However, we note that the TCPE/2013 ΔE_7 values for the less stable heptamers **CH3** and **HM1** are underestimated with respect to the quantum ones by about 2 kcal mol^{-1} , an error which is percentage wise small compared to the total interaction energies reported in Table II.

All the quantum investigations of the global minimum of the water dimer, performed using the MP2 or the CCSD level

of theory with medium up to very extended basis sets, exhibited that the dimer oxygen-oxygen distance value is $2.91 \pm 0.01 \text{ \AA}$ (see Refs. 2 and 24, for instance). Unlike the water dimer, the oxygen-oxygen distances in larger water clusters are much more sensitive to the quantum level of theory used. For instance, the mean inter-oxygen distance in the cyclic water trimer varies from 2.78 to 2.84 \AA when considering optimizations performed at the MP2/aug-cc-pVQZ level of theory and at the CCSD/aug-cc-pVDZ one, respectively.⁴² This *a priori* prevents a reliable comparison between TCPE/2013

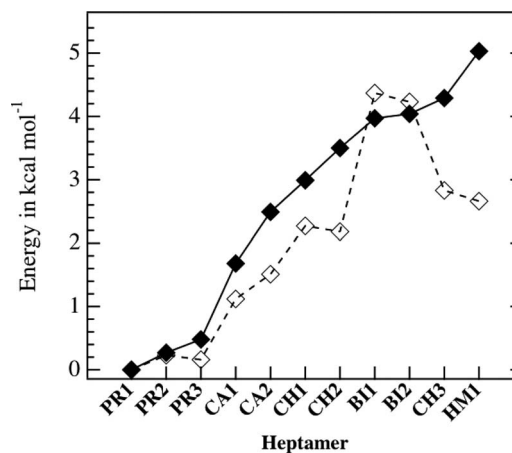


FIG. 3. Water heptamer energies ΔE_7 , the reference is here the most stable water heptamer **PR1**. The heptamer labelling corresponds to that of Temelso *et al.*²⁸ (Empty squares) TCPE/2013 results. (Full squares) Quantum estimates at the CCSD(T)/CBS level taken from Ref. 28.

TABLE III. Comparison of TCPE/2013, quantum MP2/aug-cc-pVTZ² and TTM2-F² mean oxygen-oxygen distances, in Å, in small cyclic water clusters.

$(\text{H}_2\text{O})_n$	TCPE	MP2	TTM2-F
2	2.906	2.907	2.899
3	2.829	2.787	2.800
4	2.810	2.732	2.765
5	2.780	2.716	2.750
6	2.754	2.707	2.746

predictions and quantum ones for the water cluster geometries in terms of oxygen-oxygen distance. Nevertheless, we summarize in Table III these mean distances in cyclic water clusters, from the trimer to the hexamer, computed according to TCPE/2013, as well as the distances reported by Burnham *et al.*,² computed both at the MP2/aug-cc-pVTZ level of theory and by using their accurate water model TTM2-F. We note the TCPE/2013 distances to be in good agreement with the TTM2-F ones, however, both sets of model distances are slightly overestimated compared to the MP2 ones.

2. Interaction energies for water molecules in cation first hydration shell

In Figure 4, we plot the difference in the water repulsive interaction energies occurring in the Th(IV) first hydration shell, between the TCPE/2008 and TCPE/2013 models and our own MP2/CBS computations, as a function of the number N_w of repulsively interacting water molecules ($N_w = 3-10$, the quantum results are presented in details in the supplementary material⁸³). For TCPE/2008, that difference increases linearly with N_w as soon as $N_w = 4$, up to reach a value of 25 kcal mol⁻¹ for $N_w = 10$, whereas, with TCPE/2013, that difference is almost constant, about 5 kcal mol⁻¹ for $5 \leq N_w \leq 9$, and very small for $N_w = 10$, about 1 kcal mol⁻¹. Hence, one of the goal of the TCPE/2013 development is satisfactorily reached.

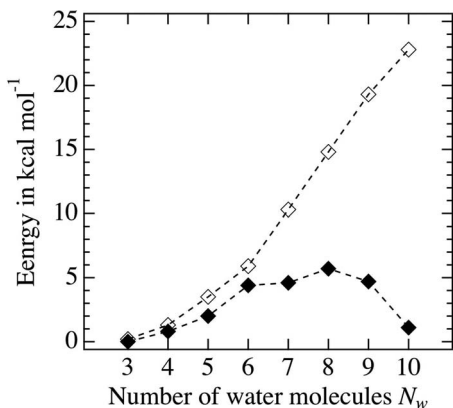


FIG. 4. Differences in water repulsive interaction energies in Th(IV) first hydration shell, between TCPE models and MP2/CBS quantum computations, as a function of the number N_w of the repulsively interacting water molecules. (Empty squares) Differences computed from TCPE/2008 results. (Black squares) Differences computed from TCPE/2013 results.

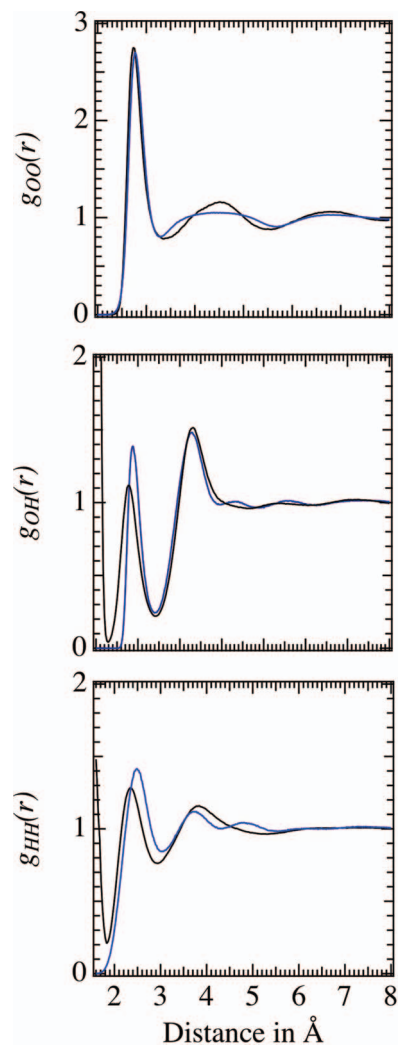


FIG. 5. Water radial distribution functions $g_{OO}(r)$, $g_{OH}(r)$, and $g_{HH}(r)$ at ambient conditions. Blue line: TCPE/2013; black line: experimental data of Soper.⁴³

B. Water in liquid phase

1. Water liquid structure

In Figure 5, we compare the radial distribution functions $g_{OO}(r)$, $g_{OH}(r)$, and $g_{HH}(r)$ at ambient conditions, computed from a 9 ns TCPE/2013 trajectory to the experimental ones reported by Soper.⁴³ The latter ones are widely used to assess the quality of a water model. For oxygen-oxygen distances smaller than 3.4 Å, the main properties of the TCPE/2013 $g_{OO}(r)$ agree with the most recent experimental data reported by Skinner *et al.*,⁴⁴ see Table IV. Note, however, that there is still controversies concerning the experimental g_{OO} first peak properties, see, for instance, the values for the first peak position and height recommended in a recent review of Nilsson and Pettersson,⁴⁵ which differ noticeably from those reported by Skinner *et al.*⁴⁴

Concerning the $g_{OO}(r)$ second peak properties, there is an experimental consensus concerning its height, $h_{max}^2 = 1.12 \pm 0.02$, and its positions, at 4.50 ± 0.02 Å (see the Soper's experimental data⁴³ plotted in Figure 5). Even though TCPE/2013 locates correctly the position of that second peak,

TABLE IV. TCPE/2013 and experimental main properties of the normalized liquid water radial distribution function g_{OO} at ambient conditions. r_m^l : position of the g_{OO} extremum l , in Å (m is the nature of the extremum); h_m^l : height of the g_{OO} extremum l ; n_c^l : coordination number at the g_{OO} minimum l .

	TCPE	Exp ^a	Exp ^b
r_{max}^1	2.785	2.80	2.82–2.85
h_{max}^1	2.70	2.57	2.1–2.3
r_{min}^1	3.28	3.45	≈ 3.5
h_{min}^1	0.80	0.84	≈ 0.9
n_c^1	4.25	4.3 ^c	
r_{max}^2	4.45	4.50	
h_{max}^2	1.06	1.12	
n_c^2	24.5	22.4 ^c	

^aExp: recommended experimental values, by Skinner *et al.*⁴⁴

^bExp: recommended experimental values, by Nilsson and Pettersson.⁴⁵

^cExp: data derived from Ref. 43.

it predicts a smaller values for its height h_{max}^2 , about 1.06, 5% smaller than the experimental estimate. However, as TCPE predicts a larger spread for that second peak compared to experiment, our theoretical estimate of the water coordination number in the second hydration shell still agrees with experiment, 24.5 and 22.4, respectively. At the exception of TTM3-F[3] we have to note that none of the most recent polarizable water models is able to accurately reproduce the experimental properties of the $g_{OO}(r)$ second peak. For instance, the model DDP2[4] also noticeably underestimates h_{max}^2 compared to experiment, while the models HBB2-pol,⁵ TTM2-F,⁴⁶ and BK3⁷ locate the second peak position 0.25 Å farther or shorter compared to experiment.

Concerning the oxygen-hydrogen radial distribution function $g_{OH}(r)$, TCPE/2013 predicts a higher and more sharpened first peak, as almost all the water models presented to date (see, among others, Refs. 4–7, 46, and 48). At the difference of the $g_{OO}(r)$, TCPE/2013 predicts accurately the $g_{OH}(r)$ second peak properties (position, height, and spread) as reported by Soper.⁴³ However, it predicts the existence of a $g_{OH}(r)$ small third peak located at about 4.5 Å, never reported experimentally and theoretically. To our opinion, it has to result from the anisotropic short range potential energy term U^{hb} , which is still not fully negligible at the latter distance. Finally, concerning the water hydrogen-hydrogen radial distribution function $g_{HH}(r)$, we note a larger discrepancy between TCPE/2013 and experiment compared to the functions $g_{OO}(r)$ and $g_{OH}(r)$. In particular, we still note the presence of $g_{HH}(r)$ third peak at about 5 Å, not reported experimentally and theoretically, with the exception of the water model BK3.⁷ However, the functions $g_{OH}(r)$ and $g_{HH}(r)$ are still considered as rather undetermined experimentally,⁴⁵ as shown by the larger experimental error bars reported for them as compared to $g_{OO}(r)$,⁴³ for instance. Moreover, accurate $g_{OH}(r)$ and $g_{HH}(r)$ functions have to be computed from simulations accounting for nuclear quantization.^{3,46,47} Hence, it is not obvious to further discuss the TCPE/2013 and experiment discrepancies concerning these functions.

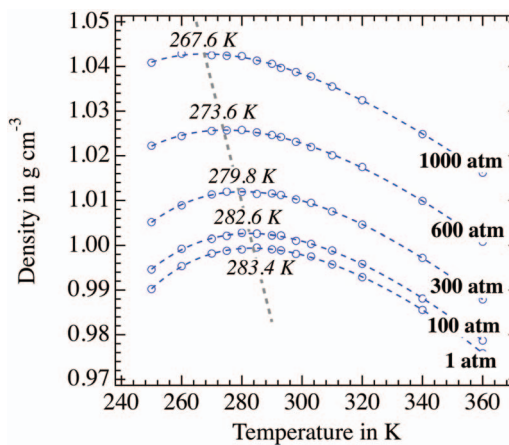


FIG. 6. TCPE/2013 liquid water densities under different temperature and pressure conditions (empty circle). For each pressure value, the result of a density fit to a 5th order polynomial function of the temperature is shown in dashed blue line. In italic, the temperatures of the density maxima. In dashed gray line, result of the linear regression of the density maxima vs. the latter temperatures.

2. Water liquid densities

As expected from our parameter assignment strategy, TCPE/2013 is able to reproduce accurately the density of liquid water at ambient conditions, e.g., 0.997 g cm^{-3} . Moreover, the model is also able to predict the existence of density maxima for liquid water, for P ranging from 1 to 1000 atm. To locate the temperature $T_{max}^{\rho}(P)$ corresponding to those maxima, we adjusted the TCPE/2013 densities at a reference pressure P to a 5th order polynomial function. The water densities, their polynomial fits and the estimates of $T_{max}^{\rho}(P)$ are shown in Figure 6. At $P = 1 \text{ atm}$, the TCPE/2013 estimate of T_{max}^{ρ} is 283.5 K, about 6 K above the experimental estimate computed from the same fitting procedure, 277.8 K. Moreover, TCPE/2013 predicts $T_{max}^{\rho}(P)$ to decrease as P increases, to reach a value of 267.6 K at $P = 1000 \text{ atm}$, still in a reasonable agreement with the estimate extrapolated from sound speeds experiments, about 255 K.^{49,50} In particular, the magnitude of the density maxima depends almost linearly on the temperature T_{max}^{ρ} for $P = 1\text{--}1000 \text{ atm}$, in agreement with the latter experimental estimate.

The TCPE/2013 magnitudes of the water liquid density are in a good agreement with the experimental ones, in a large temperature domain. In the supplementary material,⁸³ we plot the difference in the water densities between TCPE/2013 and experiment for T included within 250 and 360 K, and $P = 1 \text{ atm}$. In that temperature range, TCPE/2013 densities differ from experiment by 0.5% on average, and at most by 1.9% at the highest temperatures. The good agreement between the TCPE/2013 and experimental water liquid densities leads to a good agreement between theory and experiment for the thermal coefficient α_P (their profiles are plotted vs. the temperature for $P = 1\text{--}1000 \text{ atm}$ in Figure 7). For instance, at ambient conditions, TCPE/2013 predicts α_P to be $1.9 \times 10^{-4} \text{ K}^{-1}$, in good agreement with the experimental estimate, $2.6 \times 10^{-4} \text{ K}^{-1}$. Moreover, as the experimental data, the TCPE/2013 α_P s can be accurately represented by a

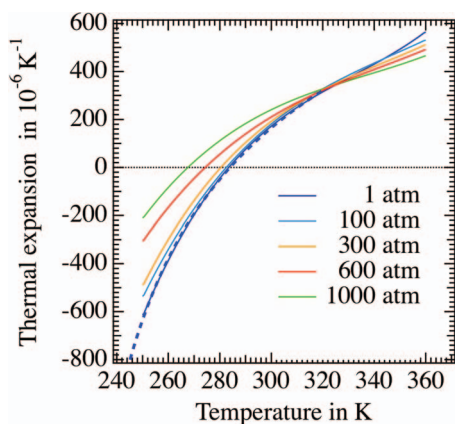


FIG. 7. TCPE/2013 water thermal expansivity for different pressure conditions. (Dashed line) Fit of α_P , for $P = 1$ atm, to the power law-based function $a_\alpha/(T - T_0^\alpha)^{\mu_\alpha}$.

singular power law function $a_\alpha/(T - T_0^\alpha)^{\mu_\alpha}$, with $T_0^\alpha = 219 \pm 4$ K and $\mu_\alpha = 0.28 \pm 0.07$.

The TCPE/2013 compressibilities κ_T under different pressure conditions are plotted as a function of the temperature in Figure 8. These values are affected by large uncertainties, representing up to 5% of the mean κ_T magnitude. However, we note that the TCPE/2013 value of κ_T at ambient conditions agrees with experiment: about $45 \pm 2 \times 10^6$ bar $^{-1}$, the experimental value is 45.3×10^6 bar $^{-1}$.⁵¹ Moreover, TCPE/2013 predicts κ_T to present a minimum at about 320 ± 10 K, regardless the pressure, as well as to decrease as the pressure increases, regardless of temperature. The TCPE/2013 κ_T behavior fully agrees with experiment.^{50,51} In particular, the magnitude of κ_T at 320 K decreases from about 45 to 35×10^6 bar $^{-1}$ when P increases from 1 atm to 1000 atm, in perfect agreement with experimental estimate reported so far.⁵¹

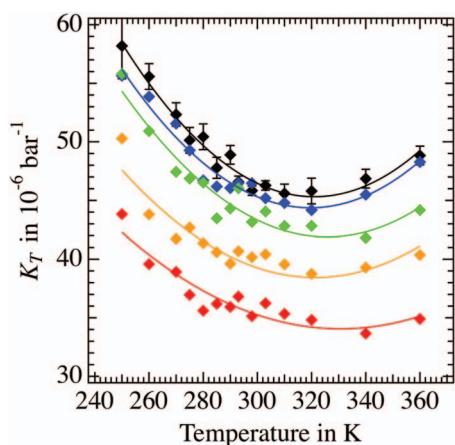


FIG. 8. TCPE/2013 isothermal compressibilities κ_T under different pressure conditions. Black symbols: $P = 1$ atm; blue symbols: $P = 100$ atm; green symbols: $P = 300$ atm; orange symbols: $P = 600$ atm; red symbols: $P = 1000$ atm. (Lines) Second order polynomial functions best reproducing the κ_T values for each pressure condition.

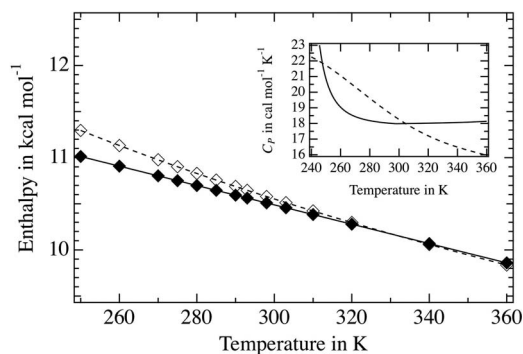


FIG. 9. Water vaporization enthalpy ΔH_{vap} as a function of the temperature T , at $P = 1$ atm. Full squares: Experimental data; empty squares: TCPE/2013 data. (Inset) Heat capacity C_P (dashed line: TCPE/2013; full line: experiment).

3. Thermodynamic properties of liquid water and vapor pressure

In Figure 9, we plot the TCPE/2013 and experimental water vaporization enthalpies, ΔH_{vap} , and the heat capacities, C_P , as functions of the temperature, at $P = 1$ atm. Concerning the vaporization enthalpy, the theoretical values agree with experiment not only at ambient conditions, as expected from our assignment parameter strategy, however, also in the full temperature domain included within 250 and 360 K. The difference in the vaporization enthalpy between the model and experiment decreases as the temperature increases, from $+0.4$ kcal mol $^{-1}$ at 250 K towards being negligible at 360 K.

Contrary to experiment, TCPE/2013 predicts C_P to be a decreasing function of the temperature for T included within 270 and 360 K. However, the difference in the C_P values between TCPE/2013 and experiment is small, at most 2 cal mol $^{-1}$ K $^{-1}$ (about 10% of the C_P value) at the boundaries of the latter temperature domain, and about 1 cal mol $^{-1}$ K $^{-1}$ on average. Note that we do not account here for the standard corrections arising from the quantum and classical contributions of the intramolecular vibrational modes, as our model is rigid. However, as the quantum correction is -2.2 cal mol $^{-1}$ K $^{-1}$ at ambient conditions,⁵² the conclusion concerning the TCPE/2013 accuracy in computing C_P still holds. In particular, as the recent BK3 model, TCPE/2013 is not able to reproduce the experimental profile of C_P , especially in the supercooled regime, where the TCPE/2013 decreasing character of C_P vs the temperature is less pronounced compared to experiment.^{53,54} This artifact may result from the classical framework we used to simulate supercooled water, as discussed recently by Vega *et al.*⁵⁵

The Gibbs free energy values, $\Delta G_{vap}(T)$, computed for $P = 1$ atm, are summarized in Table V and they are plotted as a function of the temperature T in Figure 10. In the temperature range included within 310 and 400 K, $\Delta G_{vap}(T)$ depends linearly on T . A linear fit of $\Delta G_{vap}(T) = a_G + b_G T$ gives $a_G = 10.34 \pm 0.09$ kcal mol $^{-1}$ and $b_G = -27.01 \pm 0.25$ cal mol $^{-1}$ K $^{-1}$. Both values agree reasonably well with experimental $\Delta H_{vap}(T)$ and $\Delta S_{vap}(T)$ data, see Table V. Moreover, they allow us to estimate the water boiling point T_{boil} , e.g., the temperature for which $\Delta G_{vap}(T_{boil}) = 0$. From the latter a_G and b_G coefficients, we obtain $T_{boil} = 383 \pm 5$ K, in good

TABLE V. Computed and experimental Gibbs free energy and related data. Temperatures are in K, the thermodynamic data ΔG and ΔH in kcal mol⁻¹, ΔS in cal mol⁻¹ K⁻¹, and pressures in atmospheres. Experimental data, labelled by the superscript ^{exp}, are taken from Ref. 80.

T	ΔG_{sim}	ΔG_{vap}	P_{vap}	ΔH_{vap}	ΔS_{vap}	ΔH_{vap}^{exp}	ΔS_{vap}^{exp}	P_{vap}^{exp}
310	6.41	1.97	0.041	10.42	27.26	10.38	27.96	0.062
320	6.30	1.68	0.071	10.30	26.94	10.28	27.65	0.105
340	6.05	1.11	0.196	10.06	26.32	10.07	27.02	0.272
360	5.87	0.60	0.433	9.84	25.67	9.86	26.44	0.622
380	5.70	0.13	0.844	9.62	24.97	9.65	25.89	1.282
400	5.41	-0.46	1.787	9.42	24.75	9.39	25.235	2.42

agreement with the experimental value, 373 K. Note that we do not consider here the free energy corrections proposed by Horn *et al.*,⁵⁶ as our approach is rigid and polarizable.

4. Electrostatic and dielectric properties of liquid water

The mean molecular dipole moment for water in liquid phase, $\bar{\mu}$, is predicted by TCPE/2013 to be 2.51 ± 0.01 D at ambient conditions. That value is underestimated by about 20% compared to the value estimated from experimental data using a mean-field approach.⁵⁷ However, it lies within the limiting values commonly reported when simulating liquid water with polarizable models (the limiting values are 2.4 and 2.8 D, see Refs. 6, 46, 58, and 59, for instance). At $P = 1$ atm, $\bar{\mu}$ decreases as the temperature increases (see the plot summarized in the supplementary material⁸³), until to reach a value of 2.45 D at 360 K. The incidence of the pressure is small on the latter $\bar{\mu}$ values, we note at most an increase of 0.01 D when comparing the values computed at $P = 1$ and 1000 atm.

In Figure 11, we plot the dielectric constant ϵ_r of liquid water as a function of the temperature (within 270 and 360 K), for $P = 1$ and 1000 atm. Even though these values are here computed over long trajectory segments, they are still affected by large uncertainties, which can be as large as 5% of the computed values. Nevertheless, in agreement with experiment, we note that the computed ϵ_r values depend linearly

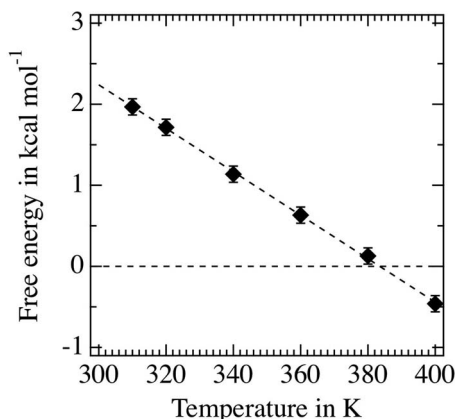


FIG. 10. Water Gibbs free energy ΔG_{vap} computed from TCPE/2013, as a function of the temperature, for $P = 1$ atm. In dashed line, the linear regression fit.

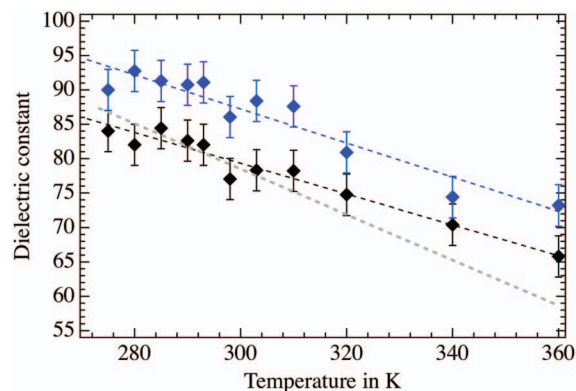


FIG. 11. Dielectric constant ϵ_r of liquid water. Black squares: TCPE/2013 ϵ_r computed at $P = 1$ atm; blue squares: TCPE/2013 ϵ_r computed at $P = 1000$ atm. (Dashed lines) Linear regression of the TCPE/2013 data (the corresponding regression coefficients are larger than 0.996 for both sets of ϵ_r values). (Bold gray line) Linear regressions of experimental values of ϵ_r under a pressure of 1 atm.

on the temperature, regardless of the pressure. Moreover, for $P = 1$ atm, the TCPE/2013 estimates of ϵ_r are in good agreement with experiment,⁶⁰ especially in the temperature domain included within 270 and 320 K. For instance, at $T = 298$ K, TCPE/2013 predicts ϵ_r to be 77 ± 3 , whereas the corresponding experimental value is 78.4. For temperatures higher than 320 K, TCPE/2013 predicts slightly overestimated ϵ_r values compared to experiment, at most by 10% at 360 K.

Regardless of temperature, the TCPE/2013 ϵ_r values increase almost linearly with pressure, at a mean rate of 0.08 atm^{-1} (see the data summarized in the supplementary material⁸³). However, because of the uncertainties affecting the computed ϵ_r values, the latter rate is only a crude estimate. Experimentally, ϵ_r is also reported to increase as the pressure increases, however, twice as fast as in our simulations (see the data collected in Ref. 60).

In Figure 12, we plot the Debye dielectric relaxation time τ_D as a function of the temperature. As the dielectric constant ϵ_r , the values of τ_D are affected by large uncertainties for temperatures smaller than 290 K, uncertainties which can be as large as 25% of the τ_D values. Nevertheless, our computed τ_D values are in good agreement with experiment.^{61–63}

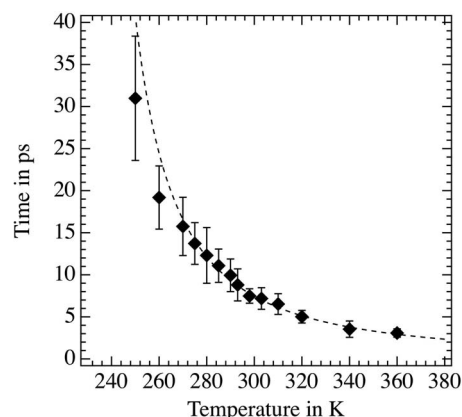


FIG. 12. Debye dielectric relaxation time τ_D computed from exponential fits of the simulation cell total dipole moment auto-correlation functions.

For instance, at ambient conditions, TCPE/2013 predicts τ_D to be 7.5 ± 1.2 ps, a value very close to the experimental one, 8.2 ± 0.4 ps.⁶¹ As expected from the agreement between TCPE/2013 and experiment, the fit (on the temperature domain 280–360 K) of the TCPE/2013 τ_D values to the power law function $a_D/(T - T_0^D)^{\mu_D}$ provides a set of T_0^D and μ_D values in very good agreement with the experimental ones, namely, 231 ± 18 K and 1.5 ± 0.4 for TCPE/2013. Experimentally, T_0^D ranges from 228 to 235 K and μ_D ranges from 1.55 to 1.79.^{63–65}

5. Mean residence time in first water hydration shell

The water mean residence times, mrt_s , in the water first coordination shell are plotted as a function of $1/T$ in Figure 13. Three sets of mrt values have been computed according to the Impey approach:³⁷ they correspond to the parameter τ^* , used in Eq. (31), set to 1, 2, and 4 ps, respectively. The uncertainties affecting the mrt_s are at most of 2%.

Regardless of the temperature, the mrt_s increase as τ^* increases. For instance, at ambient conditions, the mrt is 3.0, 3.4, and 4.2 ps, for $\tau^* = 1, 2,$ and 4 ps, respectively. These values agree with all the theoretical data reported to date, which are included within 3 and 9 ps.³⁸ Moreover, the mrt is an increasing function of the inverse of the temperature T , and that behavior is not tied to the value of the parameter τ^* . In particular, the mrt follows a non-Arrhenius behavior at low temperatures, regardless of τ^* . The magnitudes and the latter remarkable feature of our own computed mrt_s agree with the residence time magnitudes and behavior estimated from NMR experiments.⁶⁶ Moreover, as several liquid water properties, our computed mrt_s can also be accurately represented by a power law function $a_{mrt}/(T - T_0^{mrt})^{\mu_{mrt}}$, with $T_0^{mrt} = 219 \pm 6$ K and $\mu_{mrt} = 1.45 \pm 0.15$, regardless of τ^* (see the supplementary material⁸³).

6. Dynamical properties of liquid water

From the water coefficients of diffusion D_{sim} computed for different water box dimensions L and at dif-

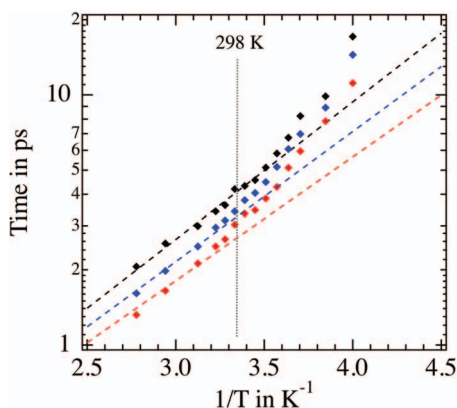


FIG. 13. Water mean residence times, mrt_s , in the water first coordination shell, computed from the Impey approach,³⁷ with the parameter τ^* set to 1 ps (red squares), 2 ps (blue squares), and 4 ps (black squares). The linear regression fits of the latter set of mrt_s as a function of $1/T$ are shown in dashed lines. They are computed by considering only mrt values corresponding to temperatures within 298 and 340 K.

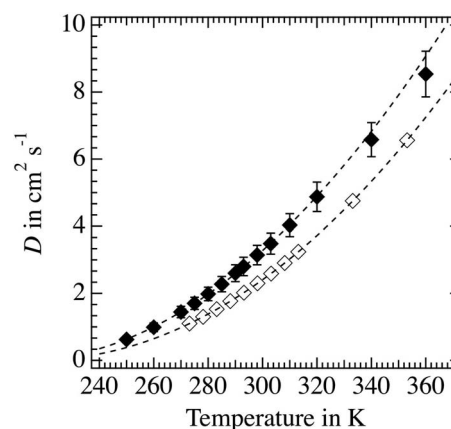


FIG. 14. TCPE/2013 (dark symbols) and experimental (empty symbols) diffusion coefficients as a function of the temperature. (Dashed line) Fit to a power law function.

ferent temperatures, we estimated the diffusion coefficient $D_\infty(T)$ and the shear viscosity $\eta(T)$ according to the relation (24) (the computed data are provided in the supplementary material⁸³). The D_∞ values are plotted as a function of the temperature in Figure 14. These values are overestimated by 40% compared to experiment for temperatures greater than 280 K. For instance, at ambient conditions, D_∞ is $3.6 \pm 0.5 \times 10^{-5} \text{ cm}^2 \text{ s}^{-1}$, whereas the experimental value is $2.6 \times 10^{-5} \text{ cm}^2 \text{ s}^{-1}$. However, the D_∞ trend is close to the experimental one. For instance, we fitted the D_∞ s to the power-law function $a_D/(T - T_0^D)^{\mu_D}$. We obtain 219 ± 6 K and 1.8 ± 0.1 for T_0^D and μ_D , respectively, in good agreement with the parameters derived from the experimental data: 215 ± 1 K and 2.06 ± 0.05 , respectively.⁶⁷

The TCPE/2013 shear viscosities $\eta(T)$ are clearly underestimated compared to experiment for $T < 310$ K, by about 40%. For instance, at ambient conditions, the TCPE/2013 η is 0.51 cp, whereas the experimental value is 0.89 cp.⁶⁸ However, the difference in η values between experiment and TCPE/2013 decreases as T increases, until to be negligible at $T = 360$ K ($\eta = 0.29$ cp experimentally and for TCPE/2013).

The former TCPE/2008 model was able to predict values for D_∞ and η in better agreement with experiment ($3.0 \pm 0.5 \times 10^{-5} \text{ cm}^2 \text{ s}^{-1}$ and 0.75 cp at ambient conditions, unpublished data). To our opinion, the less accurate estimates computed from TCPE/2013 concerning both the latter dynamical properties originate from our new parameter assignment strategy, which leads to noticeably weaken the water oxygen-oxygen repulsive interactions as compared to the former TCPE/2008 model (see Sec. II C).

C. Water at the liquid/vapor interface

The plots showing the TCPE/2013 water densities $\rho(z)$ in the direction orthogonal to the air/liquid interface at various temperatures are provided in the supplementary material.⁸³ By defining classically the thickness δl of the air/liquid interface as the region where the water density varies from 95% to 5% of the bulk one, the TCPE/2013 δl values are about 4, 6, and 10 Å at $T = 300, 400,$ and 550 K, respectively. At

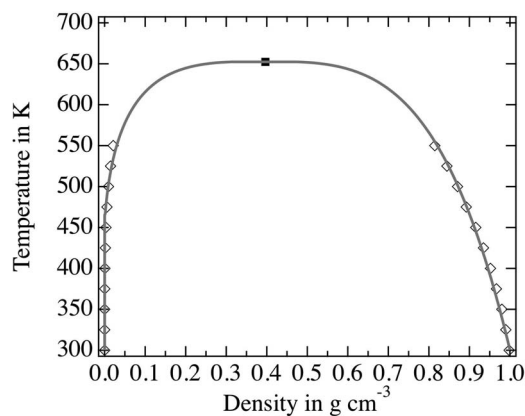


FIG. 15. Equilibrium vapor/liquid densities (shown in empty squares). (Black square) Critical point location.

$T = 300$ K, our computed δl value agrees with all the theoretical values reported to date, see Ref. 69, for instance. The profiles $\rho(z)$ have been fitted to the function defined in Eq. (33), and the fitted values corresponding to the water liquid and vapor densities ρ_l and ρ_v are reported in Figure 15.

From the densities ρ_l and ρ_v , which are denoted below ρ_+ and ρ_- , we locate the water critical point using the standard procedure based on the Wegner expansion in power of the quantity $|T - T_c|$,⁷⁰ limited to its first three terms

$$\rho_{\pm} = \rho_c + b_0|T - T_c| \pm (b_1|T - T_c|^{\beta_e} + b_2|T - T_c|^{\beta_e+1/2}), \quad (35)$$

the subscript c refers to the critical point, b_0 , b_1 , and b_2 are three adjustable parameters. Here, we set the parameter β_e to the universal value determined from the renormalization group theory, e.g., 0.325. The fitted critical temperature T_c and the critical density ρ_c are in particularly good agreement with experiment: the TCPE/2013 ones are 653 ± 14 K and 0.394 ± 0.005 g cm⁻³, respectively, whereas they are 647 K and 0.322 g cm⁻³ experimentally. If we consider our estimates of T_c and ρ_c together with our crude estimate of the critical pressure P_c , about 250 atm (see Sec. IV B 3), all these results demonstrate the ability of TCPE/2013 to describe the air/water liquid interface over a large temperature range.

Finally, we plot in Figure 16 the experimental and TCPE/2013 water surface tension, $\gamma(T)$, for temperatures included within 250 and 550 K. The difference between TCPE/2013 and experimental data are at most of 10% for temperatures smaller than 360 K. However that difference decreases as the temperature increases up to be negligible for temperatures around 400 K. As compared to the recent model BK3,⁷ whose parameters are mainly developed to reproduce a large set of liquid water properties, the TCPE/2013 predictions for $\gamma(T)$ appear to be even of better quality, especially for temperatures larger than 400 K.

From the accurate experimental measurements of Hacker⁷¹ and as recently rediscussed by Holten *et al.*,⁵⁰ $\gamma(T)$ presents an inflection point at about 268 K. Even though our estimates of γ are affected by large uncertainties in the supercooled regime, the trend of our computed data seem also to show the existence of an inflection point at about 270 K. We may note here that, from a MD simulation study based on a

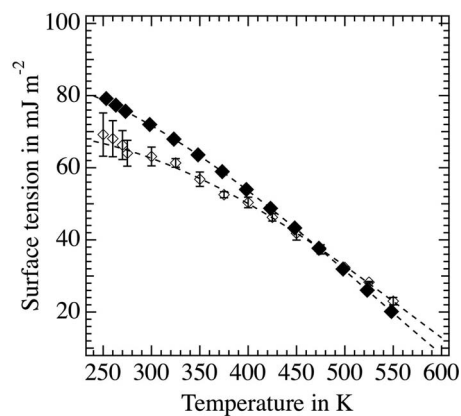


FIG. 16. Surface tension of liquid water. (Black squares) Experimental data from Refs. 71 and 79. (Empty squares) TCPE/2013 results. (Dashed lines) Results of the fit to the equation defined Eq. (36).

pairwise water model, Lü and Wei⁷² showed the existence of an inflection point for γ as well, however, at a higher temperature (about 303 K). Moreover, their computed $\gamma(T)$ exhibits a stronger dependence on the temperature in the supercooled regime as compared to experiment and to our computations.

An alternative route to estimate the temperature T_c of the water critical point is to fit the water surface tension to the function proposed by Vargaftik *et al.*⁷³

$$\gamma(T) = a_\gamma(T_c - T)^{5/4} + b_\gamma(T_c - T)^{9/4}, \quad (36)$$

for temperatures greater than 275 K. Here, a_γ and b_γ are two parameters. By adjusting the latter parameters and the critical temperature T_c to our simulation results, we obtain $a_\gamma = 0.063 \pm 0.003$, $b_\gamma = -6.7 \pm 0.8 \times 10^{-5}$, and $T_c = 675 \pm 7$ K, in agreement with those derived from the experimental data: $a_\gamma = 0.071 \pm 0.001$, $b_\gamma = -6.9 \pm 0.02 \times 10^{-5}$, and $T_c = 647.0 \pm 0.1$ K. In particular, the present TCPE/2013 estimate of T_c agrees with the above estimate computed from the TCPE/2013 densities ρ_l and ρ_g , about 653 ± 13 K.

Finally, we also estimated the pressure P_c of the water critical point by fitting the pressure P_{vap} , computed according to Eq. (23), to the Antoine relation

$$\ln P_{vap} = a_P + \frac{b_P}{c_P + T}, \quad (37)$$

where, a_P , b_P , and c_P are three adjustable parameters. By fitting them to the data corresponding to temperatures within 320 and 400 K, we obtain $P_c = 250 \pm 50$ atm, in good agreement with experiment, about 221 atm.⁷⁴

TCPE/2013 is thus able to predict several properties of liquid water on a wide range of temperature, in particular, the properties of the water critical point, with a particular high level of accuracy.

V. CONCLUSION

We propose here a revised version of the original TCPE/1997 model, e.g., TCPE/2013, which is shown to provide a good description of water systems, from gas phase clusters to bulk liquid water, as well as the air/liquid water interface, on a wide range of temperatures and pressures.

Moreover, and even though the revised model still slightly overestimates the water repulsive interactions occurring in cation first hydration shell, the error is now drastically reduced compared to all the efficient water models used up to now to investigate the solvation of cations. This demonstrates the ability of TCPE/2013 to be used to simulate neat water, as well as salt aqueous solutions and ions at the air/liquid water interface.

Contrary to all the recent models proposed to accurately model water systems, TCPE/2013 only considers a single polarizable center per water molecule, a key point in terms of computational efficiency. For instance, for a typical water box made of 1000 molecules simulated using periodic boundary conditions, the SPME approach and the multiple time steps algorithm r-RESPAP,¹⁷ the cost of the polarization treatment represents 35% of the total computational time needed to perform a MD simulation. Note that we consider here a tight convergence criterion for the dipole moments, which insures a good total energy conservation along the trajectories. Moreover, the sophisticated energy terms U^{hb} and U_{rep}^{hb} represent 12.5% and 2.5%, respectively, of the latter total computational time. These performances allow us to perform routinely, on modern supercomputing systems, numerically accurate and expensive computations, like free energy ones, as well as to simulate much larger systems on large enough time intervals.

The TCPE approach considers an energy term, here $U^{hb} + U_{rep}^{hb}$, which is strongly tied to the microscopic properties of water hydrogen bonding. This could be an interesting feature to investigate the relation between water hydrogen bond network properties and water anomalies, as discussed recently by Mallamace *et al.*⁷⁵ In particular, we note that TCPE/2013 predicts a temperature, about 225 ± 5 K, at which several properties of liquid water in the supercooled regime have to diverge (such as the thermal expansivity and the Debye relaxation time), in agreement with the analyses of experimental data.^{51,54,75,76} Hence, even though TCPE/2013 was developed to reproduce solely properties of water clusters in gas phase and of liquid water at ambient conditions, the latter result suggests that it could also be also usefully considered to investigate the properties of supercooled water, for instance, in conjunction with the theoretical analysis framework proposed by Limmer and Chandler.^{77,78} However, as TCPE/2013 considers the water molecules as rigid, it is not suited to be used to investigate phenomena tied to the anharmonic character of water OH bonds, like the water isotopic fractionation.⁸¹

However, some room still exists to improve the quality of the model TCPE/2013, in particular, to better reproduce water dynamical properties such as the diffusion coefficient and the shear viscosity. As a set of four TCPE/2013 parameters have been assigned arbitrarily, one may consider to assign them in order to meet the experimental values of the latter properties. Moreover, we may also consider alternative analytical functions to model the incidence of the surrounding environment on the local properties of a hydrogen bond. However, since its first stage of development, the main objective of the TCPE approach is to best reproduce quantum data concerning water aggregates in gas phase, as computed at a quantum high level of theory (in particular, now, at the complete basis set

limit). As the available computational resources continue to increase at a fast rate, we consider that more and more, and obviously larger and larger, water clusters will be investigated at a quantum high level of theory in a near future. These new data will help us in developing a “first principle” TCPE-based water model. Nevertheless, the model TCPE/2013 is already well suited to investigate the solvation of ions and of salts in aqueous phase, under different physical conditions and in different environments. It has to be noted that the transferability of the TCPE approach to other kind of hydrogen bonded systems (like alcohol and mixed alcohol/water ones) has already been shown for clusters.⁸² We have also already combined the TCPE/2008 model (to handle water interactions) with sophisticated models to handle anion/water and heavy ion/water interactions^{14,15,19} (the latter ion/water models are also based on many-body potentials, whose analytical form is close to the water U^{hb} one). The main difficulties to efficiently combine a TCPE water model with such ion/water potentials arises from building/updating specific atom neighbor lists (one for each kind of energy term).

ACKNOWLEDGMENTS

We thank Othman Bouizi and Emmanuel Oseret (Exascale Computing Research Laboratory, a joint INTEL/CEA/UVSQ/GENCI laboratory) for their help in optimizing the code POLARIS(MD). All the MD simulations have been performed on the supercomputing center CCRT (Centre de Calcul et de Recherche Technologique) of the French Nuclear Agency (CEA). We also acknowledge computer access to the cluster of the PhLAM institute. We gratefully acknowledge use of the Fusion cluster in the Laboratory Computing Resource Center at Argonne National Laboratory.

- ¹P. T. Kiss and A. Baranyai, *J. Chem. Phys.* **137**, 084506 (2012).
- ²S. Xantheas, J. Burnham, and R. Harrison, *J. Chem. Phys.* **116**, 1493 (2002).
- ³G. Fanourgakis and S. Xantheas, *J. Chem. Phys.* **128**, 074506 (2008).
- ⁴R. Kumar, F.-F. Wang, G. Jenness, and K. Jordan, *J. Chem. Phys.* **132**, 014309 (2010).
- ⁵V. Babin, G. Medders, and F. Paesani, *J. Phys. Chem. Lett.* **3**, 3765 (2012).
- ⁶W. Yu, P. Lopes, B. Roux, and A. MacKerell, Jr., *J. Chem. Phys.* **138**, 034508 (2013).
- ⁷P. T. Kiss and A. Baranyai, *J. Chem. Phys.* **138**, 204507 (2013).
- ⁸K. Tielrooij, N. Garcia-Araez, M. Bonn, and H. Bakker, *Science* **328**, 1006 (2010).
- ⁹R. Netz and D. Horinek, *Annu. Rev. Phys. Chem.* **63**, 401 (2012).
- ¹⁰T.-M. Chang and L. X. Dang, *Chem. Rev.* **106**, 1305 (2006).
- ¹¹P. Jungwirth and D. J. Tobias, *Chem. Rev.* **106**, 1259 (2006).
- ¹²J. Noah-Vanhoucke and P. Geissler, *Proc. Natl. Acad. Sci. U.S.A.* **106**, 15125 (2009).
- ¹³C. Caleman, J. Hub, P. van Maaren, and D. van der Spoel, *Proc. Natl. Acad. Sci. U.S.A.* **108**, 6838 (2011).
- ¹⁴F. Réal, M. Trumm, B. Schimmelpfennig, M. Masella, J.-P. Flament, and V. Vallet, *J. Phys. Chem. B* **114**, 15913 (2010).
- ¹⁵F. Réal, M. Trumm, B. Schimmelpfennig, M. Masella, and V. Vallet, *J. Comput. Chem.* **34**, 707 (2013).
- ¹⁶M. Masella and J.-P. Flament, *J. Chem. Phys.* **107**, 9105 (1997).
- ¹⁷M. Masella, *Mol. Phys.* **104**, 415 (2006).
- ¹⁸C. Houriez, N. Feéré, M. Masella, and D. Siri, *J. Chem. Phys.* **128**, 244504 (2008).
- ¹⁹M. Trumm, Y. O. Guerrero Martínez, F. Réal, M. Masella, V. Vallet, and B. Schimmelpfennig, *J. Chem. Phys.* **136**, 044509 (2012).
- ²⁰B. Thole, *Chem. Phys.* **59**, 341 (1981).

- ²¹K. Ichikawa, Y. Kameda, T. Yamaguchi, H. Wakita, and M. Misawa, *Mol. Phys.* **73**, 79 (1991).
- ²²F. Keutsch and R. Saykally, *Proc. Natl. Acad. Sci. U.S.A.* **98**, 10533 (2001).
- ²³R. Bukowski, K. Szalewicz, G. C. Groenenboom, and A. van der Avoird, *J. Chem. Phys.* **128**, 094313 (2008).
- ²⁴G. Tschumper, M. L. Leininger, B. C. Hoffman, E. F. Valeev, H. F. Schaefer III, and M. Quack, *J. Chem. Phys.* **116**, 690 (2002).
- ²⁵B. Smith, D. Swanton, J. Pople, H. Schaefer III, and L. Radom, *J. Chem. Phys.* **92**, 1240 (1990).
- ²⁶S. Xantheas and E. Apra, *J. Chem. Phys.* **120**, 823 (2004).
- ²⁷R. Shields, B. Temelso, K. Archer, T. Morell, and G. Shields, *J. Phys. Chem.* **114**, 11725 (2010).
- ²⁸B. Temelso, K. Archer, and G. Shields, *J. Phys. Chem. A* **115**, 12034 (2011).
- ²⁹T. Yang, S. Tsushima, and A. Suzuki, *J. Phys. Chem. A* **105**, 10439 (2001).
- ³⁰R. E. Wilson, S. Skanthakumar, P. C. Burns, and L. Soderholm, *Angew. Chem., Int. Ed.* **46**, 8043 (2007).
- ³¹M. Mazars, *Phys. Rep.* **500**, 43 (2011).
- ³²A. Toukmaji, C. Sagui, J. Borad, and T. Darden, *J. Chem. Phys.* **113**, 10913 (2000).
- ³³Y. Liu and M. E. Tuckerman, *J. Chem. Phys.* **112**, 1685 (2000).
- ³⁴G. J. Martyna, M. E. Tuckerman, D. J. Tobias, and M. L. Klein, *Mol. Phys.* **87**, 1117 (1996).
- ³⁵M. R. Shirts and V. S. Pande, *J. Chem. Phys.* **122**, 134508 (2005).
- ³⁶I.-C. Yeh and G. Hummer, *J. Phys. Chem. B* **108**, 15873 (2004).
- ³⁷R. W. Impey, P. A. Madden, and I. R. McDonald, *J. Phys. Chem.* **87**, 5071 (1983).
- ³⁸D. Laage and J. T. Hynes, *J. Phys. Chem. B* **112**, 7697 (2008).
- ³⁹G. Gloor, G. Jackson, F. Bias, and E. de Miguel, *J. Chem. Phys.* **123**, 134703 (2005).
- ⁴⁰C. Vega and E. de Miguel, *J. Chem. Phys.* **126**, 154707 (2007).
- ⁴¹M. Masella, N. Gresh, and J.-P. Flament, *J. Chem. Soc., Faraday Trans.* **94**, 2745 (1998).
- ⁴²I. Nielsen, E. Seidl, and C. Janssen, *J. Chem. Phys.* **110**, 9435 (1999).
- ⁴³A. Soper, *Chem. Phys. Lett.* **258**, 121 (2000).
- ⁴⁴L. Skinner, C. Huang, D. Schlesinger, L. Petterson, C. Nilsson, and A. qnd Benmore, *J. Chem. Phys.* **138**, 074506 (2013).
- ⁴⁵A. Nilsson and L. Pettersson, *Chem. Phys.* **389**, 1 (2011).
- ⁴⁶F. Paesani, S. Iuchi, and G. Voth, *J. Chem. Phys.* **127**, 074506 (2007).
- ⁴⁷G. S. Fanourgakis, G. K. Schenter, and S. S. Xantheas, *J. Chem. Phys.* **125**, 141102 (2006).
- ⁴⁸Y. Wu, H. L. Tepper, and G. Voth, *J. Chem. Phys.* **124**, 024503 (2006).
- ⁴⁹R. Speedy, *J. Phys. Chem.* **86**, 982 (1982).
- ⁵⁰V. Holten, C. Bertrand, M. Anisimov, and J. Sengers, *J. Chem. Phys.* **136**, 094507 (2012).
- ⁵¹G. Kell, *J. Chem. Eng. Data* **20**, 97 (1975).
- ⁵²A. Glitli, X. Daura and W. van Gunsteren, *J. Chem. Phys.* **116**, 9811 (2002).
- ⁵³C. Angell, J. Shuppert, and J. Tucker, *J. Phys. Chem.* **77**, 3092 (1973).
- ⁵⁴E. Tombari, C. Ferrari, and G. Salvetti, *Chem. Phys. Lett.* **300**, 749 (1999).
- ⁵⁵C. Vega, M. M. Conde, C. McBride, J. L. F. Abascal, E. G. Noya, R. Ramirez, and L. M. Sesé, *J. Chem. Phys.* **132**, 046101 (2010).
- ⁵⁶H. W. Horn, W. Swope, and J. Pitera, *J. Chem. Phys.* **123**, 194504 (2005).
- ⁵⁷A. Gubskaya and P. Kusalik, *J. Chem. Phys.* **117**, 5290 (2002).
- ⁵⁸O. Akin-Ojo and K. Szalewicz, *J. Chem. Phys.* **138**, 024316 (2013).
- ⁵⁹G. Lamoureux, A. MacKerell, and B. Roux, *J. Chem. Phys.* **119**, 5185 (2003).
- ⁶⁰*CRC Handbook of Chemistry and Physics*, 68th ed., edited by D. Lide (CRC Press, 1994).
- ⁶¹J. Kindt and C. Schmittenmauer, *J. Phys. Chem.* **100**, 10373 (1996).
- ⁶²C. Ronne, L. Thrane, P. O. Strand, A. Wallqvist, K. V. Mikkelsen, and S. R. Keiding, *J. Phys. Chem.* **107**, 5319 (1997).
- ⁶³C. Ronne, P. O. Strand, and S. Keiding, *Phys. Rev. Lett.* **82**, 2888 (1999).
- ⁶⁴R. Speedy and C. Angeli, *J. Chem. Phys.* **65**, 851 (1976).
- ⁶⁵*Water: A Comprehensive Treatise*, edited by F. Franks (Plenum Press, New York, 1981).
- ⁶⁶J. Teixeira, *Mol. Phys.* **110**, 249 (2012).
- ⁶⁷M. Holz, S. Heil, and A. Sacco, *Phys. Chem. Chem. Phys.* **2**, 4740 (2000).
- ⁶⁸L. Korson, W. Drost-Hansen, and F. Millero, *J. Phys. Chem.* **73**, 34 (1969).
- ⁶⁹Y. Fan, X. Chen, L. Yang, P. Cremer, and Y. Gao, *J. Phys. Chem. B* **113**, 11672 (2009).
- ⁷⁰F. Wegner, *Phys. Rev. B* **5**, 4529 (1972).
- ⁷¹B. Hacker, "Experimental values of the surface tension of supercooled water," Technical Note 2510 (National Advisory Committee for Aeronautics, 1951).
- ⁷²Y. Lü and B. Wei, *Appl. Phys. Lett.* **89**, 164106 (2006).
- ⁷³N. Vargaftik, B. Volkov, and L. Voljak, *J. Phys. Chem. Ref. Data* **12**, 817 (1983).
- ⁷⁴See <http://www.webbook.nist.gov/chemistry/fluid> for NIST webbook.
- ⁷⁵F. Mallamace, C. Corsaro, and H. Stanley, *Proc. Natl. Acad. Sci. U.S.A.* **110**, 4899 (2013).
- ⁷⁶P. Debenedetti and H. Stanley, *Phys. Today* **56**(6), 40 (2003).
- ⁷⁷D. Limmer and D. Chandler, *J. Chem. Phys.* **135**, 134503 (2011).
- ⁷⁸D. Limmer and D. Chandler, *J. Chem. Phys.* **138**, 214504 (2013).
- ⁷⁹M. Floriano and C. Angell, *J. Phys. Chem.* **94**, 4199 (1990).
- ⁸⁰W. Wagner and A. Pruss, *J. Phys. Chem. Ref. Data* **31**, 387 (2002).
- ⁸¹T. E. Markland and B. J. Berne, *Proc. Natl. Acad. Sci. U.S.A.* **109**, 7988 (2012).
- ⁸²M. Masella and J.-P. Flament, *Mol. Phys.* **95**, 97 (1998).
- ⁸³See supplementary material at <http://dx.doi.org/10.1063/1.4821166> for cluster geometries, details of simulation results, and of quantum computations.